HYDROLOGICAL PROCESSES
Hydrol. Process. **22**, 3980–3997 (2008)
Published online 16 July 2008 in Wiley InterScience
(www.interscience.wiley.com) DOI: 10.1002/hyp.7085

A study of the energy balance and melt regime on Juncal Norte Glacier, semi-arid Andes of central Chile, using melt models of different complexity

Francesca Pellicciotti,[1]* Jakob Helbing,[2] Andrés Rivera,[3] Vincent Favier,[4] Javier Corripio,[5] José Araos,[6] Jean-Emmanuel Sicart[7] and Marco Carenzo[1]

[1] *Institute of Environmental Engineering, Federal Institute of Technology, ETH-Hoenggerberg, CH-8093, Zurich, Switzerland*
[2] *Swiss Federal Institute of Aquatic Science and Technology (Eawag), Zurich, Switzerland*
[3] *Centro de Estudios Cientificos (CECS), Valdivia, Chile*
[4] *Centro de Estudios Avanzados en Zonas Aridas (CEAZA), La Serena, Chile*
[5] *Institute of Geography, University of Innsbruck, Austria*
[6] *Centro de Estudios del Cuaternario, Fundación CEQUA, Punta Arenas, Chile*
[7] *Great Ice Unit, Institut de la Recherche pour le Development (IRD), Montpellier, France*

Abstract:

We use meteorological data from two automatic weather stations (AWS) on Juncal Norte Glacier, central Chile, to investigate the glacier–climate interaction and to test ablation models of different complexity. The semi-arid Central Andes are characterized by dry summers, with precipitation close to zero, low relative humidity and intense solar radiation. We show that katabatic forcing is dominant both on the glacier tongue and in the fore field, and that low humidity and absence of clouds cause strong radiative cooling of the glacier surface. Surface albedo is basically constant for snow and ice, because of the scarcity of solid precipitation. The energy balance of the glacier is simulated for a 2-month period in austral summer using two models of different complexity, which differ in the inclusion of the heat conduction flux into the snowpack and in the parameterization of the incoming longwave radiation. Net shortwave radiation is the dominant component of the energy balance. The sensible heat flux is always positive, while both the net longwave radiation and latent heat flux are negative. Neglecting the subsurface heat flux and corresponding variations in surface temperature leads to an overestimation of ablation of 2% over a total of 3695 mm water equivalent (w.e.) at the end of the season. Correct modelling of incoming longwave radiation is crucial, and we suggest that parameterizations based on vapour pressure and air temperature should be used rather than on computed cloud amount. We also used an enhanced temperature-index model incorporating the shortwave radiation flux, which has two empirical parameters. We apply it both with values of parameters obtained for Alpine glaciers and recalibrated on Juncal Norte. The model recalibrated against the correct energy balance simulations performs very well. The model parameters respond to the meteorological conditions typical of this climatic setting. Copyright © 2008 John Wiley & Sons, Ltd.

KEY WORDS energy balance; ablation models; temperature-index modelling; Juncal Norte; semi-arid Andes

Received 29 September 2007; Accepted 30 April 2008

INTRODUCTION

The semi-arid Andes of central Chile are characterized by a pronounced seasonality, with water in summer originating mainly from snow and glacier melt (Peña and Nazarala, 1987; Masiokas and others, 2006), and precipitation basically absent (Figure 1) (Pellicciotti and others, 2007). Both agriculture and urban centres of growing demographic and economic importance rely on melt water for their summer supply and there is increasing competition for water allocation as water uses increase with growing population and the country's industrialization (Cai and others, 2003; Masiokas and others, 2006; Rivera and others, 2006).

A number of recent studies have provided evidence of glacier retreat and thinning in central Chile during the twentieth century (Rivera and others, 2000, 2002), showing that a general glacier recession has occurred, with an average estimate of 12·8% of area loss in the 51 years from 1945 to 1996 (Rivera *et al*., 2002). Results of temperature trend analysis in the whole region (Carrasco *et al*., 2005) and specifically in the upper Aconcagua River Basin (Pellicciotti and others, 2007) agree in pointing to a statistically significant increase in both summer and winter air temperature in the last decades. A sustained positive change in air temperature is likely to affect both the summer snowmelt, by enhancing it, and the phase of the winter precipitation, decreasing the amount of snow accumulated at the onset of the melt season (Masiokas and others, 2006). Carrasco and others (2005) have shown an increase of the elevation of the snow line in central Chile in the last quarter of the twentieth century by 127 m.

This area, therefore, being so crucially dependent on glaciers and snowcovers for its water supply, is much vulnerable to possible climatic changes. These, however,

* Correspondence to: Francesca Pellicciotti, Institute of Environmental Engineering, Federal Institute of Technology, ETH-Hoenggerberg, CH-8093, Zurich, Switzerland. E-mail: pellicciotti@ifu.baug.ethz.ch

have been little investigated (Bown and others, 2008) and this study intends to provide a first contribution for the understanding and modelling of the effects of climatic changes on the water resources in the region. A key step in the understanding of the impact of climate change on glaciers is the study of the energy balance at the glacier-atmosphere interface and of the related ablation processes. Extensive studies of the energy balance and glacier-climate interaction have been conducted in the South American continent for the tropical Andes of Bolivia (e.g. Wagnon and others, 1999; Sicart and others, 2005) and in the inner tropics in the Ecuadorian Andes (Favier and others, 2004a, b; Francou and others, 2004). This is not the case for the semi-arid Andes of central Chile, where only a couple of works have examined issues related to the modelling of the energy balance (e.g. Corripio, 2003; Corripio and Purves, 2005). These works, however, had to cope with a limited amount of data and short period of measurements.

The main aim of this work is to investigate the glacier-climate interaction in the climatic area of the semi-arid Andes for an entire ablation season. We also intend to test ablation models of different complexity that have been developed and extensively used in the Alps in the different climatic settings of these latitudes. These are characterized by very dry and stable summers, with precipitation close to zero and low relative humidity. Solar radiation is very intense, and plays a key role in the energy balance of snow covers and glaciers. The investigation is carried out on Juncal Norte Glacier, in the upper Aconcagua River Basin north of the capital city Santiago, at the location of two automatic weather stations (AWSs) that we set up as part of a broader field campaign. There, availability of input data directly measured allows to concentrate on the analysis of processes at the point scale without the errors that are introduced by extrapolation of the meteorological variables in distributed melt modelling. In a following paper, we will address the extrapolation of the energy balance to the entire glacier and distributed modelling of the glacier ablation using a digital elevation model (DEM) of the glacier.

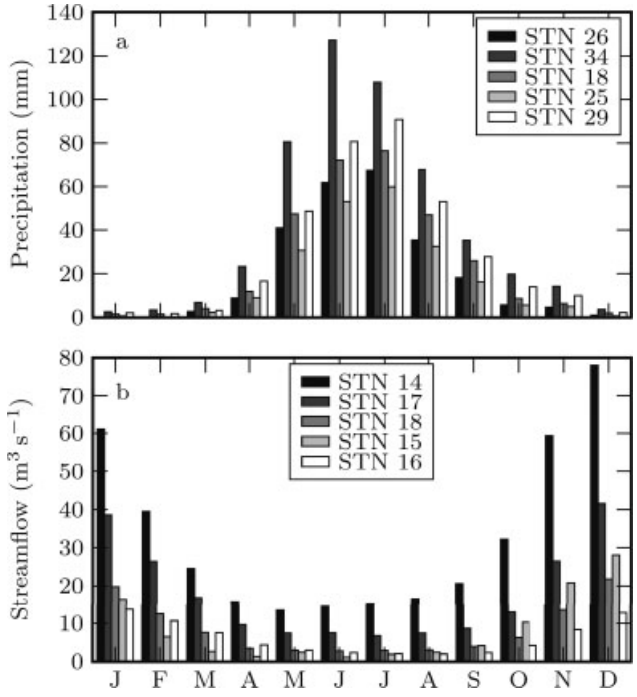

Figure 1. Mean monthly precipitation (a) and runoff (b) at a number of gauging stations (STN) in the Aconcagua River Basin, semi-arid Andes of central Chile. Mean values over the period of record 1974–2004. The position of the meteorological and streamflow stations is shown in Figure 2

According to the aims of this work, we first explore, using the meteorological data sets collected on and outside the glacier during a 2-month field campaign, the climatological regime of the area, trying to identify the processes that are typical of these latitudes in comparison to other climatic settings. We then apply two physically based energy balance models of different complexity and test their simulations against ablation measurements at both an ultrasonic depth gauge (UDG) and ablation stakes. Once the relevant physical processes have been identified through energy balance modelling, we use an enhanced temperature-index (ETI) model and apply it with both parameter values typical of the Alps and recalibrated for the local conditions.

The ETI melt model (Pellicciotti and others, 2005) was developed on a glacier in the Swiss Alps (Haut Glacier d'Arolla) and has been tested extensively in the Alps, where it proved to be able to simulate melt rates across a glacier accurately both at the point and the distributed scale (Pellicciotti, 2004; Pellicciotti and others, 2005; Rimkus, 2006; Kretz, 2007). The model has empirical parameters that need calibration and might therefore be site dependent. A recent work on the robustness and transferability of model parameters has shown that the ETI model is indeed transferable without recalibration of parameters for a number of glaciers and ablation seasons in the Alps (Carenzo and others, 2008). Here we want to evaluate its applicability to glaciers in the climatic setting of the semi-arid Andes. The model can be applied using temperature data as only measured input, as the solar radiation flux can be modelled (Pellicciotti and others, 2005), and it therefore offers, in comparison with energy balance models, less data requirement. This might be important in areas such as the semi-arid Andes where little data exist.

This study makes use of a new data set collected on Juncal Norte Glacier during a 2-month field campaign in the ablation season 2005–2006.

STUDY SITE AND DATA

Field site

Juncal Norte Glacier (32·98°S, 70·11°W) is located in the upper Aconcagua River Basin, in the semi-arid Andes of central Chile, north of the capital city of Santiago and near the Argentinean border just south of the Portillo pass (Figure 2). The glacier flows northwards

DOI: 10.1002/hyp

of Nevado Juncal peak from about 6100 to 2900 m, has an area of about 7·6 km^2 and a length of about 7·5 km (Figure 2). Between 1955 and 2003, the ablation area has experienced a thinning rate of $0{\cdot}63 \pm 0{\cdot}37$ m y^{-1} (Bown and others, 2008). Because of the relatively easy accessibility compared to most of the glaciers in the area, some data have been collected on the glacier (Corripio, 2003), but no data set available spans the whole ablation season (a period of about 10 days of meteorological measurements was recorded by Corripio (2003) in 2000) nor offers an extensive amount of different data that allow a thorough validation of models. In this sense, the data set presented here is quite unique both in terms of duration of the time series collected and amount of meteorological, geophysical, ablation, and runoff data. In this study, we concentrate on the melt regime of the ablation area because this is the zone of the glacier that is most contributing to glacier runoff.

Data

An extensive glacio-meteorological experiment was conducted on the Juncal Norte Glacier from early December 2005 to mid February 2006, spanning the entire ablation season, and a large data set was collected, including meteorological measurements, runoff and ablation observations, surface elevation data and photographs of the glacier lower part from a fixed camera.

Meteorological data. Two AWSs were installed on the glacier and in the proglacial valley in close proximity to the glacier terminus (Figure 2 and Table I). They measured 5 min records of the following meteorological variables: air temperature (°C), relative humidity (%), wind speed (m s^{-1}) and direction (°), incoming and reflected shortwave radiation (W m^{-2}). Data were sampled every 5 s and averages stored on Campbell CR10X dataloggers every 5 min. Measurements of air temperature were shielded and ventilated. The two AWSs are similar in design, with sensors fixed to an arm suspended from a mast. The main difference is that the glacier AWS sits on a tripod that stands freely on the glacier surface and sinks with it as this melts, thus allowing a constant distance between sensors and surface to be kept. The shortwave radiation sensor is therefore mounted parallel to the surface. The AWS in the proglacial valley, on the contrary, was drilled in the ground. All measurements were taken at a height of 2 m, nominal for the glacier station as the station melted slightly over the first few days until it reached equilibrium. The sensors and their specifications are listed in Table II.

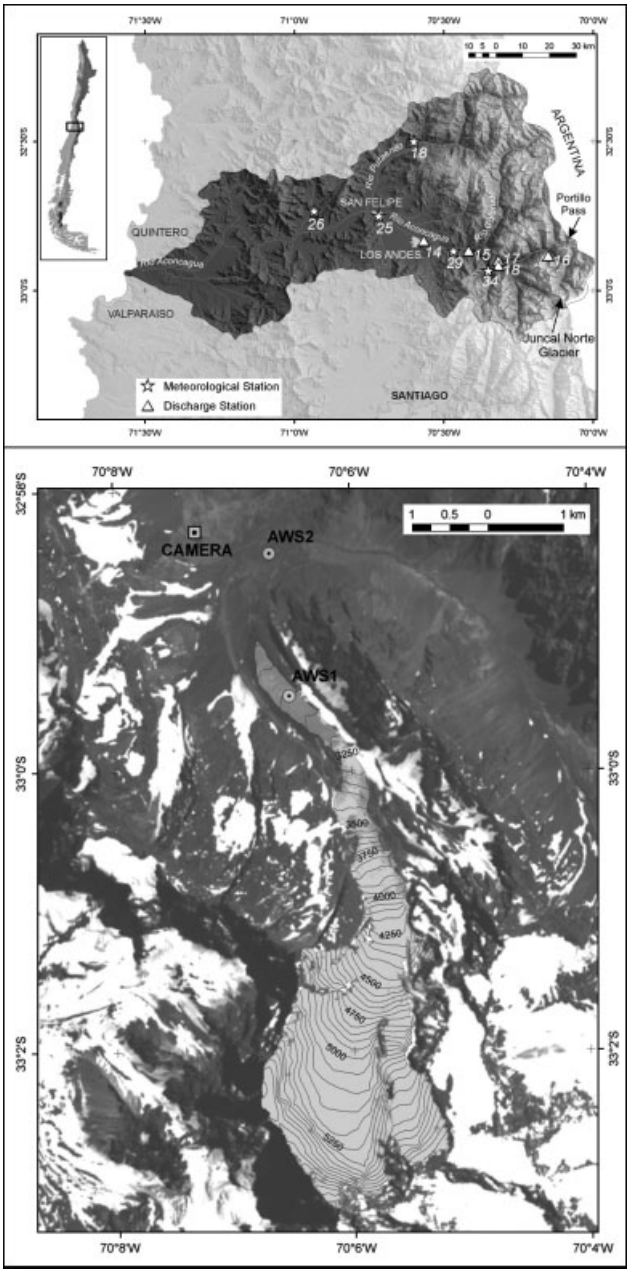

Figure 2. Top: map of the Aconcagua River Basin with the position of the meteorological and streamflow stations of Figure 1 and of Juncal Norte glacier; bottom: map of Juncal Norte Glacier showing the position of the two Automatic Weather Stations on (AWS1) and outside (AWS2) the glacier. Contour lines based upon Shuttle Radar Topography Mission (SRTM) elevation data

The glacier AWS, henceforth referred to as AWS1, was installed on the glacier tongue in the lower ablation area, close to the glacier flow line (Figure 2) on a flat surface, and is therefore representative of the surface and

Table I. Characteristics of the two automatic weather stations on and close to Juncal Norte Glacier, ablation season 2005–2006. The location refers to the position of each AWS during the ablation season 2005–2006, and was measured with differential GPS

Station	Elevation (m)	Latitude	Longitude	Location	Period of functioning
Glacier (AWS1)	3127	32° 59' 26" S	70° 06' 31" W	Ablation area	11 Dec 2005–12 Feb 2006
Proglacial (AWS2)	2811	32° 58' 27" S	70° 06' 40" W	Proglacial valley	18–23 Dec 2005, 9 Jan–14 Feb 2006

DOI: 10.1002/hyp

Table II. Meteorological sensors mounted on the two automatic weather stations on and close to Juncal Norte Glacier, and some of their technical characteristics

Variable measured	Manufacturer	Sensor	Accuracy	Range
Shortwave radiation ($Q\downarrow$ and $Q\uparrow$)	Kipp and Zonen	CM7B	±5%	305–2800 nm
Relative humidity	Rotronic	MP-103A	±1%	0–100%
Temperature	Rotronic	MP-103A	±0·3 °C	(−40) − (+60) °C
Wind speed	Young	S-WMON	±0·3 m s^{-1}	1–60 m s^{-1}
Wind direction	Young	S-WMON	±3°	—

meteorological conditions of the glacier ablation area. When the snowpack was depleted, a rough ice surface emerged, characterized by surface bumps and an extensive debris cover. The proglacial station will be referred to as AWS2 in the paper. All meteorological data were averaged into hourly means and used as input to the melt models.

Ablation data. Ablation data were obtained using two different methods. An UDG was installed at the location of AWS1, on a mast drilled into the ice. The UDG recorded continuously 5 min data of surface lowering over the period of measurement. The sensor tilted because the mast melted out of the surface on 25 January 2006, so that a time series of reliable data is available only until that date. Ablation stakes were also set up across the glacier, and three of them were drilled in the proximity of AWS1 few metres apart from each other. Readings of the stakes were made at intervals of few days in the first period and later on at intervals of few weeks. The average of the readings of the three stakes is used.

Snow density was measured in a snow pit at the beginning of the measurement period (on 9 December, 2005) at the location of AWS1, and its mean value was 524 kg m^{-3}. The mean value of the deepest layers (1 m below the surface) was about 540 kg m^{-3}. We therefore assumed, based on the values of the deeper layers measured on 9 December, a snow density value of 524 kg m^{-3} until 20 December 2005, and a value of 540 kg m^{-3} from 20 December until 9 January 2006, when ice appeared. Density of ice was assumed equal to 900 kg m^{-3}. Readings of surface lowering at the stake and UDG measurements were converted into snow or ice w.e. with the snow or ice densities, and used for the validation of the energy balance models.

METEOROLOGICAL DATA ANALYSIS AND CLIMATIC SETTING

Using the meteorological data set described in the Section above, the prevailing meteorological characteristics of the area were investigated. Unlike other regions in the Andes, such as the Andean area of Ecuador where temperature and humidity variations are not strong enough to define a pronounced seasonal regime (Favier and others, 2004a), the semi-arid Andes of central Chile are characterized by a very marked seasonality. Summer, defined as December, January and February (DJF), sees very low precipitation (Pellicciotti and others, 2007), associated with a belt of stationary high pressure over the Pacific Ocean west of South America which prevents intrusion of moisture-laden air masses to the continent (Corripio, 2003). Summer storms can occur at the higher elevations. The whole bulk of the total precipitation occurs mostly in winter (June, July, August, JJA) and in less measure in autumn (March, April and May, MAM) and spring (September, October and November, SON) (see Figure 1). A definition of the seasonality typical of the region is provided, among others, by Waylen and Caviedes (1990) and Montecinos and Aceituno (2003). Our measurements period covers the summer ablation season (see Table I), which is well defined and characterized by long periods of clear and stable weather, and the considerations below refer to this climatological period.

We first looked at the variability and characteristics of 2 m air temperature both on and close to the glacier. Figure 3 shows comparison of hourly air temperature measured at AWS1 and AWS2. It can be seen that temperature at the proglacial station (AWS2) is higher than at the glacier station (AWS1) and that it has much larger diurnal oscillations (see also Table III). This is to be expected given the role played by the glacier in dampening temperature fluctuations by reducing the daily maxima (e.g. Greuell and Böhm, 1998; Pellicciotti and others, 2005). The katabatic or glacier wind also contributes to explain the lower temperature at AWS1, because of the mass of cold air that it transports to the lower sections of the glacier along the glacier flowline (Greuell and Böhm, 1998). This effect is felt also at the location of AWS2, but is less strong there (see also discussion on katabatic wind below). The higher temperature fluctuations at AWS2 are explained by higher peak-day maxima rather than lower minima (Figure 3 and Table III). Differences between the daily temperature values at the two stations oscillate between 4 and 6 °C. Air temperature is always above 0 °C at both stations (Figure 3), unlike what is typical of ablation seasons in the Alps, which are characterized by more or less frequent spells of below zero air temperature, especially at night. In Figure 4a are depicted the mean daily fluctuations of air temperature over the entire period of record for both AWSs. Both records show a clear diurnal cycle, with less marked variations at AWS1 for the reasons explained above. The average air temperature at AWS2 over the period analysed is 12·6 °C, and exceeds the average air temperature at AWS1 by 4·5 °C.

Analysis of the solar radiation data confirms that incoming solar radiation is very intense, with values

DOI: 10.1002/hyp

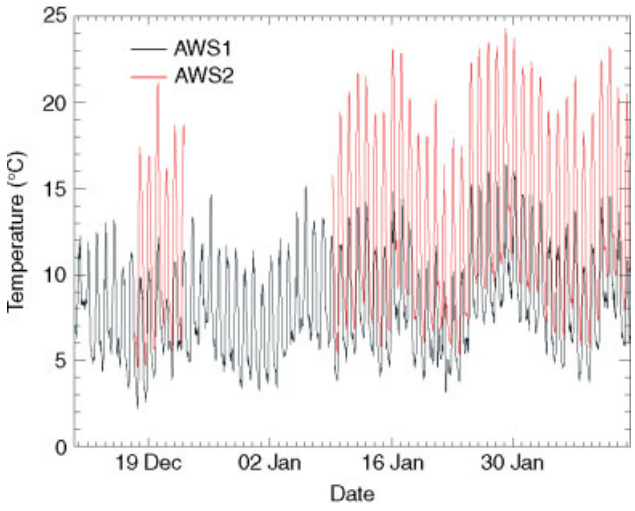

Figure 3. Comparison of hourly measurements of air temperature (°C) at the two automatic weather stations on (AWS1) and close to the glacier (AWS2). AWS2 started recording later than AWS1 and did not work in the period 23 December 2005–9 January 2006, see Table I

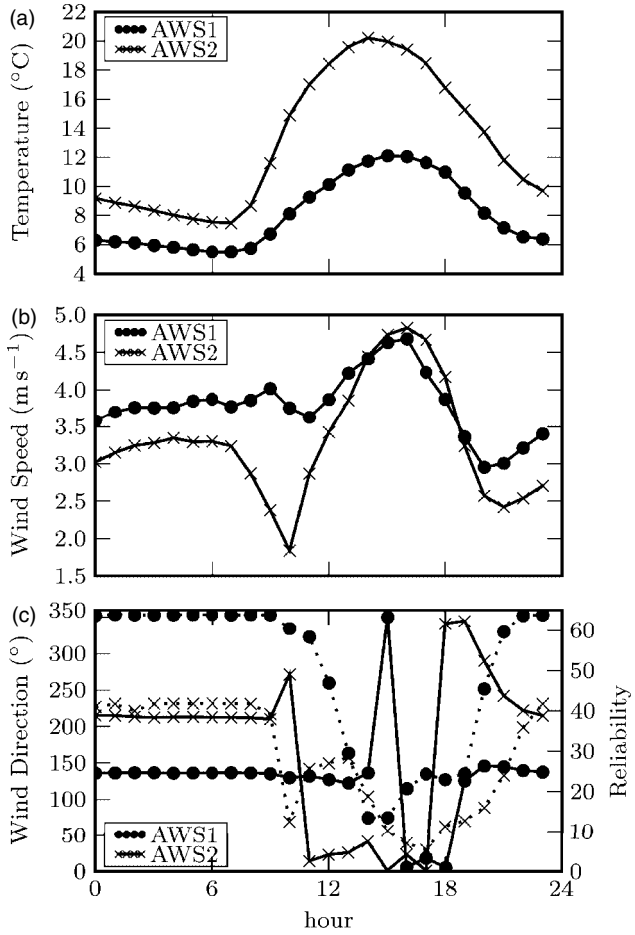

Figure 4. Mean daily fluctuations in air temperature (a), wind speed (b) and wind direction (c) at AWS1 and AWS2, averaged over the entire period of record. In the bottom plot (wind direction), continuous lines indicate wind direction (left axis) and dotted lines the reliability of the wind direction (right axis). Reliability is computed as the normalized length of the vectorial sum of the wind vectors recorded by the sensor in that hour: high values indicate persistence of same direction winds, and low values frequent changes in direction

Table III. Daily means, mean daily maxima and mean daily minima for air temperature, relative humidity and wind speed at AWS1 and AWS2. Values are computed from hourly mean data over the period of record common to both stations (see Table I)

	Air temperature °C	Wind speed m s^{-1}	Relative humidity %
AWS1			
Mean	8·1	3·8	42
Maximum	12·5	5·8	64
Minimum	5·1	2·1	21
AWS2			
Mean	12·6	3·2	34
Maximum	19·9	5·4	54
Minimum	6·8	1·5	12

almost nearing the solar constant ($I_0 = 1367$ W m^{-2}). Overcast conditions are extremely rare (see also Lliboutry, 1998), with only 4 days out of a total of 64 in the period of record characterized by cloud cover. Relative humidity on the contrary is very low (mean value for the recording period at AWS1, from 11 December 2005 to 12 February 2006, was about 42%, see Table III).

The very low summer precipitations have an important effect on the albedo of glaciers in the region, as the resetting of albedo to its peak values which is associated with snowfalls does not occur. Liquid precipitation, in contrast, would clean the surface of the ice or enhance snow metamorphism and increase its water content, but is very rare during the ablation season (Lliboutry, 1998). Figure 5 shows daily albedo at AWS1 for the period of records. It can be seen that albedo basically assumes a constant value for snow ($\alpha_{snow} \sim 0{\cdot}56$ in the first part of the record up to about 4 January) and a constant value for ice of less than 0·1 from 14 January onwards. The latter value is relatively low for ice surfaces (typical values being around 0·2–0·3, see e.g. Paterson (1994)), but it is explained by the fact that the station was sitting on a debris-covered site where supraglacial water channels were observed. Similar values for impure ice were reported by Cutler and Munro (1996) for Sonnblickgletscher. A transition period between the snow and ice covered surfaces can be observed in Figure 5, characterized by an almost linear decay from typical snow albedo values through lower values corresponding to slush and old, wet snow to the value of ice albedo. This limited albedo variability is interesting in the light of the implications it has for the modelling of the energy balance at the glacier surface, since albedo is a major control on the melt process (e.g. van de Wal and others, 1992; Favier and others, 2004a; Pellicciotti and others, 2005). The effect of the increase in albedo associated with snowfall on the melt process has been numerically demonstrated (Brock and others, 2000b). The absence of high variability simplifies the modelling exercise by reducing the need for albedo parameterizations that are able to capture the complex patterns of albedo resetting and successive decay following snowfalls that is typical

DOI: 10.1002/hyp

of the Alps and in general regions where relative humidity is higher and precipitation more frequent and intense (see e.g. Pellicciotti and others, 2005, for a picture of albedo variations at several locations across one Alpine glacier over one ablation season).

Analysis of wind direction frequency at both AWSs is shown in Figure 6 and indicates clearly that there is persistent katabatic wind at both stations (at AWS1 150° is down-glacier, and at AWS2 210° also indicates the flowline direction down-glacier, see Figure 2). Mean and maximum wind speed at AWS1 exceed those measured at AWS2 (Table III), suggesting that katabatic wind is stronger at AWS1 because this station is on the glacier tongue, whereas AWS2 is in the valley, where the effect of the glacier wind is felt, but less strongly. It is clear, however, that both AWSs are influenced by katabatic forcing, as it can be observed also in Figure 4, which depicts mean daily fluctuations in air temperature, wind speed, and wind direction averaged over the entire period of record. The maximum wind speed occurs at both stations around 16:00, and both stations exhibit diurnal variations.

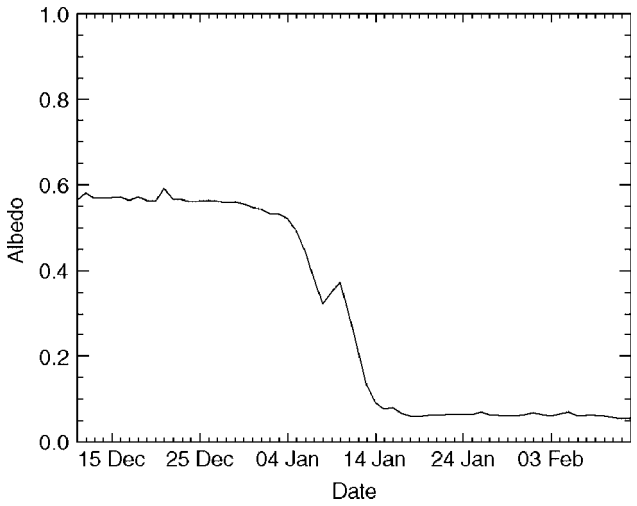

Figure 5. Daily albedo recorded at AWS1 during the period of record. Daily albedo is computed as the mean of hourly albedo values when incoming shortwave radiation is above 120 W m^{-2}

The predominant wind direction at both stations is equal to the down-glacier direction (see above) for most of the day apart from the afternoon hours, when it changes by about 180° at both stations (Figure 4c), suggesting that glacier wind is present for the entire day except the afternoon hours from 15:00 to 18:00. Analysis of reliability of the directions (normalized length of sum vector, on the right axis in Figure 4c) indicates that the glacier wind is eroded in the afternoon hours by winds of opposite direction. While the reliability of the wind direction stays very high all during the day, it drops in the afternoon hours when the wind changes direction. This seems to suggest that in the afternoon the prevailing down-glacier direction is contrasted by opposing winds, likely valley winds developing in the afternoon. Erosion of katabatic wind by the valley wind in the afternoon was observed also by Greuell and others (1997). The fact that glacier wind is observed during the whole day and not only in the afternoon hours, as it is often on Alpine glaciers, might be due to the very high air temperature of the location, which maintains a strong temperature gradient between atmosphere and glacier surface for most

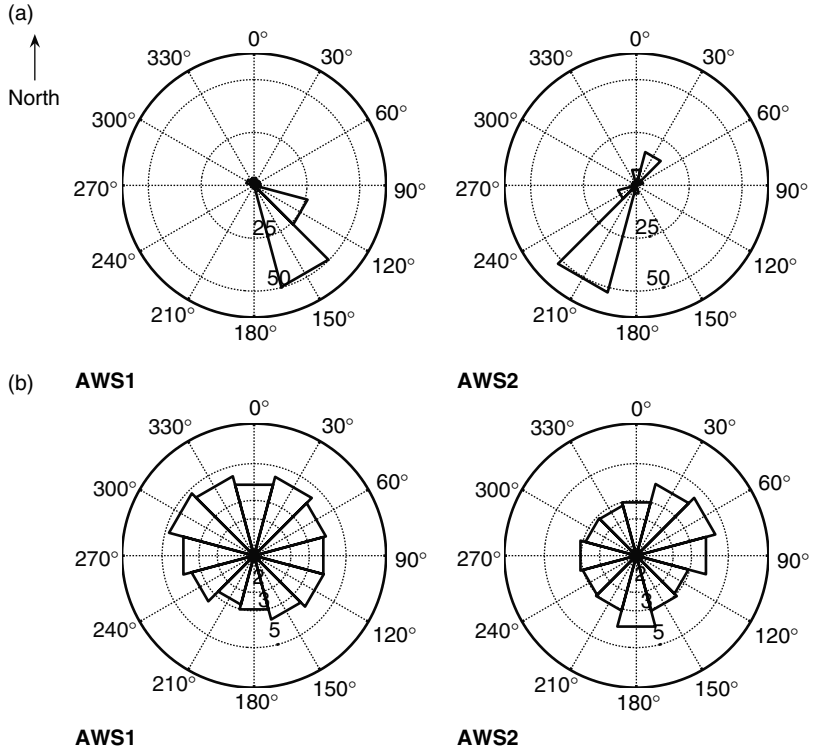

Figure 6. Distribution of 2 m hourly measurements of wind direction (a) and mean velocity (b) at AWS1 and AWS2 for the entire period of record. The frequency of wind direction is expressed as percentage over the entire season (indicated on the diagonal axes)

DOI: 10.1002/hyp

of the day. Katabatic force is created by the temperature contrast between the melting glacier surface and the ambient atmosphere, and a higher temperature contrast leads to stronger katabatic forces (Greuell and others, 1997). This is why katabatic winds are normally observed in the afternoon hours, following the hours of maximum air temperature, and why a wind-speed maximum in the afternoon is recognized as typical of glacier wind-dominated locations (e.g. van den Broeke, 1997; Greuell and Böhm, 1998; Greuell and Smeets, 2001; Klok and others, 2005).

ABLATION MODELLING

In this section, we apply ablation models of different complexity, and test their performance at the location of the AWS1, where data are available both as input to the models and for their validation. We use both physically based energy balance models and a simplified energy balance model or ETI model that includes the shortwave radiation balance (Pellicciotti and others, 2005).

Energy balance modelling

Two different energy balance models are used to simulate ablation, which mainly differ for the inclusion of the heat conduction flux into the snow and ice and for the treatment of incoming longwave radiation. The first model is the surface energy balance by Brock and Arnold (2000), henceforth referred to as EB1, in which melt is computed as residual from the energy balance equation:

$$Q_M = Q_I + L + Q_H + Q_L \quad (1)$$

where Q_M is energy available for melt, Q_I is the net shortwave radiation flux, L is the net longwave radiation flux, Q_H is the turbulent sensible heat flux and Q_L is the latent heat flux. Fluxes are assumed to be positive when directed towards the surface (e.g. Röthlisberger and Lang, 1987). No heat conduction into the snow or ice is considered, therefore assuming that the glacier is temperate and its surface is always at melting point (zero-degree assumption). In this study, the shortwave radiative flux is computed from measurements of incoming and reflected shortwave radiation at the AWS. The longwave radiation flux is modelled. Assuming that the surface is at 0 °C and radiates as a black body (emissivity equal to 1), $L\uparrow$ is a constant flux equal to -316 W m^{-2} (Oke, 1987). $L\downarrow$ is calculated from the Stefan–Boltzmann relationship

$$L\downarrow = \varepsilon^* \sigma T_a^4 \quad (2)$$

where T_a is air temperature (K), σ is the Stefan–Boltzmann constant ($5{\cdot}67 \cdot 10^{-8}$ W m^{-2} K^{-4}) and ε^* is the emissivity of the sky. This is a function of air temperature, cloud type and cloud amount (Ohmura, 1981; Arnold and others, 1996; Brock and Arnold, 2000)

$$\varepsilon^* = (1 + \kappa n)\varepsilon_0 \quad (3)$$

where ε_0, the clear-sky emissivity, is a function of air temperature (Brock and Arnold, 2000), and κ is a constant depending on cloud type (assumed to be equal to 0·26 following Braithwaite and Olesen (1990)). Cloud amount n (with $n = 1$ for complete cloud cover and $n = 0$ for a clear sky) is computed from comparison of measured incoming shortwave radiation with the modelled incoming shortwave radiation flux under a cloud-free sky (Brock and Arnold, 2000). In the original formulation, cloud amount at night was assumed to be equal to 1. In this work, we assume the cloud amount at night to be equal to the mean value of the afternoon before. This issue is discussed in more detail in the Models Application Section.

Q_H and Q_L are computed using the bulk aerodynamic method, which requires wind speed, air temperature and humidity to be measured at only one height above the surface (usually 2 m above the surface). The approach is discussed in detail in Munro (1989); Braithwaite and others (1998); Brock and Arnold (2000); Denby and Greuell (2000). The two fluxes depend additionally on the stability correction factors for momentum, heat, and humidity, the Monin–Obukhov length scale (Obukhov, 1971) and the scaling lengths for aerodynamic roughness (z_0), temperature (z_t) and humidity (z_e). In the model, z_t and z_e are computed as functions of z_0 using the roughness Reynolds number, Re^*, following Andreas (1987). The aerodynamic roughness z_0 has to be provided to the model, and its evaluation follows the scheme employed in Pellicciotti and others (2005) and used also in Carenzo and others (2008), in which three constant values of z_0 are assigned to fresh snow ($z_0 = 0{\cdot}1$ mm), snow after snowfall when melting has taken place ($z_0 = 1{\cdot}0$ mm), and ice ($z_0 = 2{\cdot}0$ mm). The three different surface types are distinguished based on field observation of the glacier surface, analysis of photographic records, air temperature and the timing of snowfalls. The values used are well in agreement with those reported in the literature (Brock and others, 2006). We also checked the sensitivity of the model simulations to these values, and obtained variations between 0·1 and 2·5% in total melt at the end of the season for variations of 10 to 90% in z_0 with respect to the original values. The highest variation (2·5%) corresponds to a simultaneous decrease of 90% for the z_0 values of both snow and ice (corresponding to an order of magnitude change in both values), while a variation of one order of magnitude for snow (from $z_0 = 1{\cdot}0$ mm to $z_0 = 0{\cdot}1$ mm, corresponding to a decrease of 90% of the original value) results in a difference in total melt of 0·8%. All energy fluxes are converted to mm w.e. by dividing by the latent heat of fusion of water ($\lambda = 0{\cdot}334$ MJ kg^{-1}).

The model has been extensively used in the Alps for simulations of ablation at the point scale (e.g. Brock and others, 2000a; Pellicciotti and others, 2005) and was recently validated over several seasons on two different glaciers in the Swiss Alps, showing a very good agreement with measurements of ablation at UDGs (Carenzo and others, 2008).

DOI: 10.1002/hyp

In the second model (Corripio, 2003), henceforth referred to as EB2, the energy fluxes at the glacier surface are expressed as:

$$Q_M = Q_I + L + Q_H + Q_L + Q_S \quad (4)$$

where Q_S is the subsurface heat flux or internal heat flux within the snow or ice, which controls the warming or cooling of the snow or ice pack. All other symbols are as in Equation (1). Q_S is computed considering the atmosphere-glacier surface-subsurface snow or ice pack as a one dimensional system (Greuell and Konzelmann, 1994; Koh and Jordan, 1995)

$$\rho_s c_s \frac{\partial T}{\partial t} = \frac{\partial}{\partial z}\left(k_s \frac{\partial T}{\partial z}\right) - \frac{\partial Q_S}{\partial z} \quad (5)$$

and using a simple two-layer subsurface model (Oke, 1987)

$$\frac{\Delta Q_S}{\Delta z} = C_s \frac{\Delta T}{\Delta t} \quad (6)$$

where ΔQ_s is the energy used to heat the snow or ice pack at the surface, and C_s is the heat capacity of the snow $C_s = \rho_s c_s$. ρ_s is snow density and c_s is the specific heat of snow ($2{\cdot}09 \times 10^3$ J kg^{-1} K^{-1}). The thermal conductivity k_s is assumed to be 0·42 for snow and 2·0715 for ice (Paterson, 1994).

The volume of snowpack affected by temperature fluctuations was estimated from the amplitude of the daily surface temperature oscillations according to Oke (1987), assuming an exponential decrease of temperature with depth (see Corripio, 2003, for details). We chose the depth corresponding to the 95% damping of the wave. Thirty six percent of the net shortwave radiation was assumed to be absorbed by the surface (following Greuell and Konzelmann, 1994), whereas the rest penetrates into the snowpack. The snow or ice pack temperature is computed from Equation (6), and is then used for computation of both the longwave radiation flux and the turbulent fluxes. The latter are computed, as in EB1, using the bulk aerodynamic method. The same z_0 values as in EB1 were used. The shortwave radiation flux is computed from measurements of incoming and reflected shortwave radiation. Incoming longwave radiation is calculated from the Stefan–Boltzmann relationship (Equation 2) using atmospheric emissivity that is function of air temperature and actual vapour pressure (Prata, 1996)

$$\varepsilon^* = 1 - (1 + w_p)e^{-(1{\cdot}2+3w_p)^{0.5}} \quad (7)$$

where precipitable water w_p is calculated following an empirical equation also given by Prata (1996) as a function of T_a and the actual vapour pressure e_0:

$$w_p = 46{\cdot}5\frac{e_0}{T_a} \quad (8)$$

This approach was demonstrated to work well for dry atmospheres (Niemelä and others, 2001). The effect of both sky obstruction and longwave emission by surrounding slopes is also taken into account in computation of the incoming longwave radiation, using the sky-view factor. Outgoing longwave radiation is computed from the Stefan–Boltzmann relationship as in EB1, with the temperature of the surface computed internally by the model from the glacier heat flux (see above). EB2 also includes computation of sublimation.

Enhanced temperature-index model

The ETI model is described in detail by Pellicciotti and others (2005), so only the main features of the model will be recalled here. In the ETI model, surface melt rate M is computed as:

$$M = \begin{cases} TF \cdot T + SRF \cdot (1-\alpha) \cdot I & T > T_T \\ 0 & T \le T_T \end{cases} \quad (9)$$

where M is the hourly melt rate (mm w.e. h^{-1}), T is air temperature (°C), α is albedo and I is incoming shortwave radiation (W m^{-2}). In the model, temperature data are measured, whereas both α and I can be either measured or parameterized. In this work, we use measured input data. The two empirical factors TF and SRF, called *temperature factor* and *shortwave radiation factor* and expressed in (mm d^{-1} °C^{-1}) and (m^2 mm W^{-2} h^{-1}), respectively, were optimized against hourly melt rates computed with an energy balance model on a Swiss Glacier (Pellicciotti and others, 2005; Carenzo and others, 2008). Their values are $TF = 0{\cdot}04$ and $SRF = 0{\cdot}0094$. The threshold temperature for melt to occur, T_T, is 1 °C (Pellicciotti and others, 2005).

One advantage of the ETI model with respect to the standard version of the approach (also known as degree-day method) is that inclusion of the shortwave radiation balance makes the model appropriate for high temporal resolution (e.g. hourly) simulations, which the classical version of the model cannot afford. In this way, we can study with all three models the diurnal variations of melt rates.

Models application

In a first step, we apply the two energy balance models for the entire period of record and test their simulations against measurements of ablation at both the stakes and UDG. Because of the nature of the ablation measurements, cumulative ablation over the entire season and not high temporal resolution melt rates are compared.

The two energy balance models differ in terms of inclusion of the subsurface heat fluxes and of computation of the incoming longwave radiative flux. In order to test the relative importance of these two model characteristics, we run two more model versions: (1) we implemented the zero-degree assumption into EB2, forcing the glacier surface to be always at melting point (thus preventing radiative cooling from occurring); (2) we tested the original model version of EB1 in which cloud amount is set to one at night (corresponding to the prescription of overcast conditions at night). In EB1, cloud amount is computed from the ratio of measured and modelled

DOI: 10.1002/hyp

clear-sky incoming solar radiation, as in several energy balance studies (e.g. Greuell and others, 1997; Greuell and Smeets, 2001; Klok and Oerlemans, 2002; Favier and others, 2004a). At night, we assume the cloud amount (also referred to as cloud factor) to be equal to the mean value of the afternoon before (see Energy Balance Modelling Section). We have used the mean value over a different number of afternoon hours with a negligible difference in modelling results. We also discarded from computation those hours when incoming shortwave radiation is defined but its values are low and errors might be caused by the low angle of the sun beam above the horizon (values below 120 W m^{-2}). Different solutions to the problem of determining cloud amount at night have been put forward by different authors, from assuming cloud cover equal to one (e.g. Brock and Arnold, 2000) to using linear interpolation (e.g. Klok and Oerlemans, 2002). In numerous studies, indeed, the choice of the cloud cover for conditions when incoming shortwave radiation is not defined is not documented. Modelling of incoming longwave radiation has been recognized as a major source of uncertainty in point-scale energy balance modelling (Greuell and Smeets, 2001), and there is agreement that most cloud cover parameterizations are not very accurate (Klok and Oerlemans, 2002). We have therefore looked at the impact of the application of a different cloud cover scheme both on the computation of the longwave radiative flux and on simulated ablation, and have therefore also computed the longwave radiative incoming flux in EB1 assuming that cloud amount at night is set to one (Brock and Arnold, 2000). This represents the case of maximum overestimation in these climatic conditions characterized by almost total absence of clouds. We then evaluated the impact of this assumption on simulated ablation. Results of these two additional model runs are reported in Table IV of the 'Results' section.

In a second step, we investigate the application of the ETI model, both by using values of empirical parameters typical of the Alps and by recalibrating them. Recalibration is conducted against the energy balance hourly simulations, using as measure of the model performance the efficiency criterion, R^2, (Nash and Sutcliffe, 1970), defined as

$$R^2 = 1 - \frac{\sum_{i=1}^{p}(M_{r_i} - M_{s_i})^2}{\sum_{i=1}^{p}(M_{r_i} - \overline{M}_{r_i})^2} \qquad (10)$$

where M is the melt rate, and the subscripts 'r' and 's' denote reference and simulated values, respectively. The bar refers to the mean, and p is the number of time steps for which R^2 is calculated. All models are applied at the hourly time scale.

Table IV. Average daily energy fluxes (W m^{-2}) at AWS1 measured or computed over the period of record by EB1, EB2 and the two model variants described in the Models Application Section: incoming (I_{in}), reflected (I_{ref}) and net (Q_I) shortwave radiation; incoming (L_{in}), outgoing (L_{out}) and net (L) longwave radiation; sensible (Q_H) and latent (Q_L) heat fluxes. Q_M is the resulting energy available for melt (Equations 1 and 4). Also reported is ablation (mass loss by melt and sublimation/evaporation): average daily ablation, M_D (mm w.e.d^{-1}), and total ablation over the entire computation period (64 days from 11 December 2007 to 12 February 2008), M_{TOT} (mm w.e.), computed by the four models. n is cloud amount, see Equation (3)

	EB1	EB2	EB2 zero-degree assumption	EB1 $n = 1$ at night
I_{in}	345	344	344	345
I_{ref}	108	106	106	108
Q_I	238	238	238	238
L_{in}	269	252	254	306
L_{out}	316	306	312	315
L	−47	−54	−58	−9
Q_H	63	56	51	63
Q_L	−34	−19	−28	−34
Q_S	—	3	—	—
Q_M	240	224	228	259
M_D	62	58	59	67
M_{TOT}	3995	3695	3770	4310

RESULTS

Energy balance simulations

Figure 7 shows comparison of cumulative ablation computed by the two energy balance models against measurements at both the UDG and ablation stake after conversion into w.e. EB2 simulations agree very well with both UDG and stake measurements over the entire period, with an almost perfect agreement on snow (up to about 15 January) and a less good match on ice. On 15 January, the snowpack disappears exposing the rough ice surface that was found at the location of AWS1. Such a surface was extremely heterogeneous, and determination of its characteristics might be affected by errors, as is the correct measurement of surface ablation at the stakes and with the UDG. In addition to this, the discrepancy might be attributed to the density used for conversion of the UDG distance readings into mm w.e., since in the transition period a mix surface could be present, with density different from the values used in this work.

EB1, on the contrary, overestimates ablation (Figure 7) from the beginning of the measurement period. The total ablation simulated by EB1 at the end of the season is 3995 mm w.e., against a total ablation computed by EB2 of 3695 mm w.e., with EB1 therefore overestimating ablation by 300 mm w.e. over a period of 64 days (see also Table IV).

Total sublimation computed by EB2 is 38 mm w.e., a relatively small amount (about 1%) compared to the total ablation. At this elevation, however, sublimation is likely to be small, and might be more important at higher elevations.

In order to understand the observed differences in cumulative ablation between EB1 and EB2, we looked

DOI: 10.1002/hyp

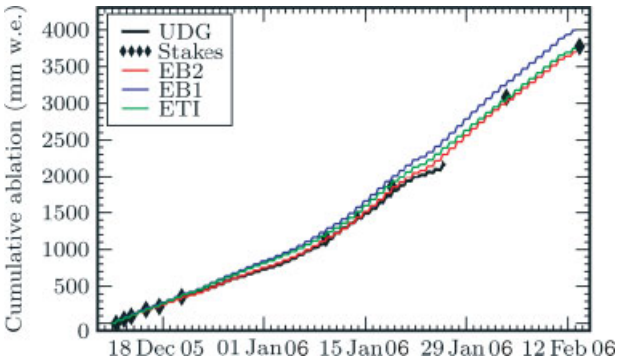

Figure 7. Comparison of cumulative ablation simulated by the two energy balance models (EB1 and EB2), by the enhanced temperature-index model (ETI), cumulative ablation recorded by the ultrasonic depth gauge (UDG) and stakes readings. Both stakes and UDG measurements were converted into mm w.e. using measured density values

at the hourly melt rates simulated by the two models. These are shown in Figure 8 for a 10-day period on snow and a 10-day period on ice, together with measurements of air temperature and incoming shortwave radiation. Ablation rates computed by both models are well correlated with both air temperature (correlation coefficient $r = 0{\cdot}724$ and $r = 0{\cdot}707$ for EB1 and EB2, respectively) and incoming shortwave radiation ($r = 0{\cdot}870$ and $r = 0{\cdot}864$, respectively). Correlation is stronger with incoming shortwave radiation, confirming evidence that the melt process at this temporal resolution is controlled by incoming shortwave radiation (e.g. Hock, 1999; Pellicciotti and others, 2005). On 21 December and 22 January, two overcast days with low temperature, both models predict low ablation, as a consequence of the much reduced solar radiation flux (Figure 8). On ice, ablation rates (as simulated by both models) are much higher than on snow (with mean peak values around 12 mm w.e. h^{-1}), because of the lower ice albedo compared to that of snow.

EB1 simulations slightly overestimate EB2 hourly ablation both on snow and ice (Figure 8c and d). In particular, overestimation occurs regularly in the first

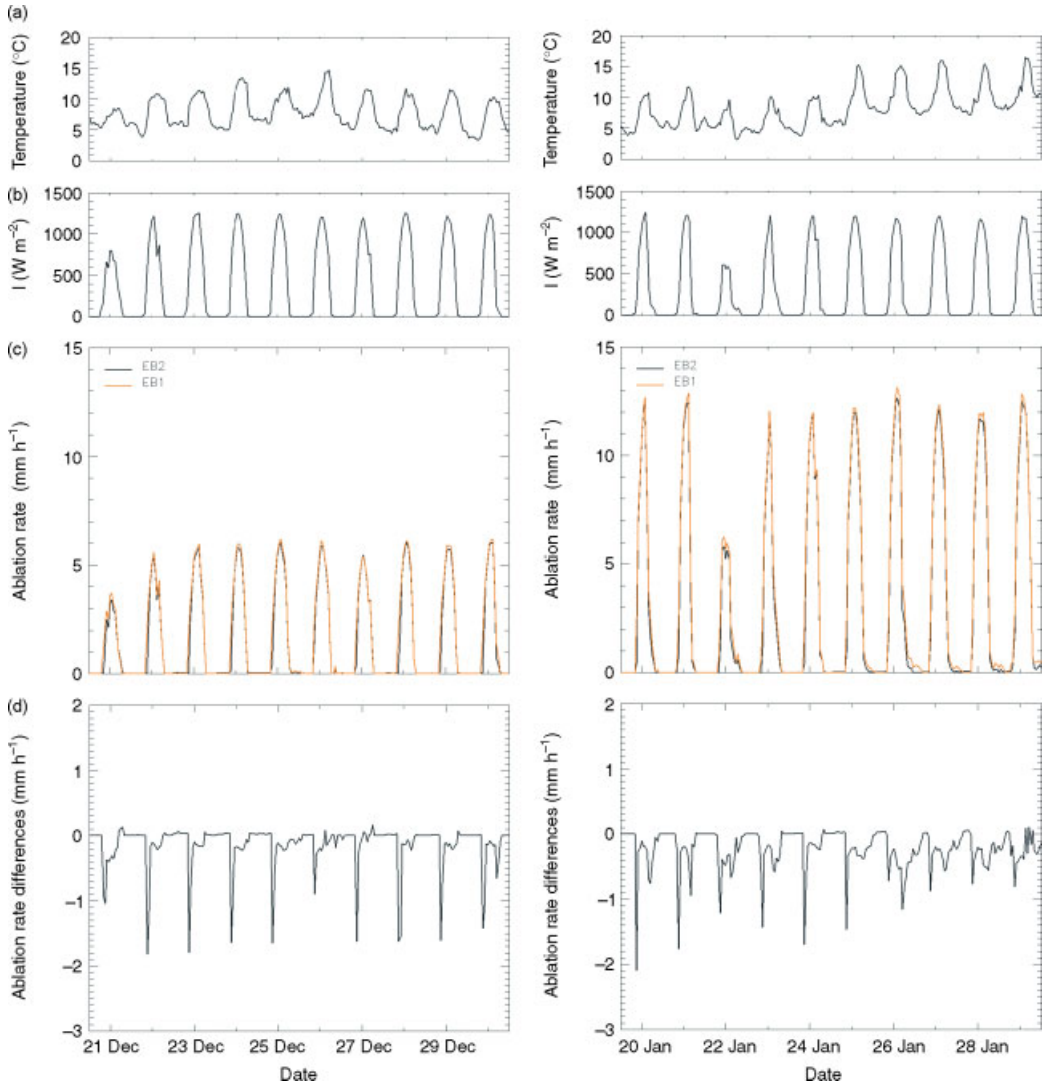

Figure 8. Measured hourly air temperature at AWS1 (a); measured incoming shortwave radiation I at AWS1 (b); hourly ablation rate simulated by EB1 and EB2 (c); and differences in hourly ablation simulated by EB1 and EB2 (d) for a 10-day period on snow, from 21 to 30 December, 2005 (left) and a 10-day period on ice, from 20 to 29 January, 2006 (right). Differences are computed as EB2-EB1

DOI: 10.1002/hyp

morning hours (Figure 8d), likely because of the zero-degree assumption, which causes EB1 to predict melt when in reality energy is used to increase the snowpack heat content to melting point. This effect is reduced when air temperature is high, especially at night, as it is observed on 25 December on snow (Figure 8a), when high air temperatures at night limit the loss of heat by the snowpack: the early morning overestimation by EB1 (indicated by the spikes in Figure 8d), is much smaller on 25 December (while some melt is predicted at night by EB1 but not by EB2).

Overestimation of ablation in the early morning hours can be observed also in EB1 simulations on ice (Figure 8c and d). Such overestimation is less pronounced on days characterized by warm air temperatures, such as the spell from 25 to 29 January (Figure 8a), when radiative cooling is less effective (Figure 8c). In the period from 25 to 29 January, air temperature is higher (both during the day and night) than in the precedent days from 20 to 24 January. In the former period, average night temperatures are around 8 °C, as compared to temperatures of about 5 °C in the latter. Under these conditions, EB1 also predicts higher ablation rates at night than EB2. Agreement between peak hours melt is very good, indicating that both models correctly reproduce the incoming shortwave radiative flux, which is the dominant forcing during day hours.

Simulations of glacier surface temperature by EB2 show that most nights the glacier surface is at temperatures below zero, as indicated in Figure 9. Surface temperatures are equal to 0 °C during the day, but drop below melting point during the night, following quite closely the behaviour of the air temperature (Figure 9). The minimum daily surface temperature, reached on average in the early morning hours before 9:00, oscillates between about −1 and −6 °C, with a minimum value of −6·4 °C (on 15 January at 7:15). Mean surface temperature over the period of record was −2·3 °C. It can be observed that periods of sustained high temperatures during the day are responsible for a less marked drop in the night temperature, as it occurs in the warm spells of 3 to 9 January and of 25 January to 4 February (Figure 9).

The assumption that the glacier surface is always at melting point causes all energy available to be used for melt, whereas in reality part of it is needed to warm up the snow or ice pack due to the strong radiative cooling taking place at nights (Wagnon and others, 1999a; Favier and others, 2004a). This explains partly the overestimation by EB1 of ablation rates, especially in the early morning hours. Analysis of the results of the EB2 model runs with and without zero-degree assumption, however, clearly indicates that most of the difference in performance between EB1 and EB2 is attributable to the parameterization used for computation of the incoming longwave radiation flux. Total ablation simulated by the model with surface temperature forced to be 0 °C is 3770 mm w.e. (Table IV), with a difference in total ablation between the two EB2 runs of 75 mm w.e. (Table IV). This suggests that the zero-degree assumption

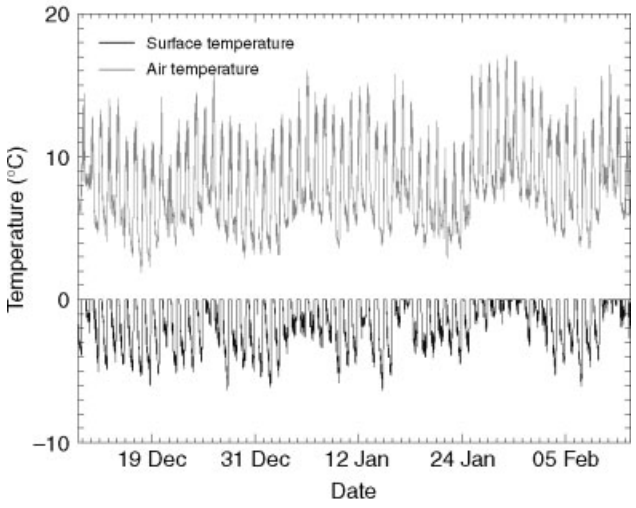

Figure 9. 5 min glacier surface temperature as modelled by EB2 (black) and 5 min air temperature measured at AWS1 (grey) over the entire period of record

is responsible for about one third of the observed overestimation of the total ablation between EB1 and EB2 (about 300 mm w.e.), the remaining part being attributable to the parameterization of incoming longwave radiation, as demonstrated by the values of the incoming longwave radiation flux listed in Table IV. The mean incoming longwave radiation flux over the period of record computed by EB1 (which assumes surface to be always at melting point) is 269 W m^{-2}, while the one calculated by EB2 with the zero-degree assumption is 254 W m^{-2}.

Inclusion of the zero-degree assumption into EB2 results in an increase in the outgoing longwave radiation from 306 to 312 W m^{-2} (Table IV), since the outgoing longwave flux is directly proportional to the absolute surface temperature, and in a related change in the net longwave radiation (from −54 to −58 W m^{-2}). It also leads to a small decrease in the sensible flux (from 56 to 51 W m^{-2}), due to the reduction of the temperature deficit that drives the sensible heat flux (e.g. Greuell and Smeets, 2001); and to an increase in the absolute value of the latent heat flux, which becomes more negative, going from −19 to −28 W m^{-2} (Table IV).

The remaining difference in total ablation between EB1 and EB2 (more than two thirds of the difference in total ablation, see Table IV) is therefore due to modelling of the incoming longwave radiation. In EB1 longwave radiation is computed as a function of air temperature and cloud amount computed as the ratio between measured and modelled clear-sky incoming shortwave radiation (Brock and Arnold, 2000). Such computation might result in an overestimation of overcast conditions, because even small differences in modelled and measured incoming shortwave radiation result in the prediction of cloud conditions, as demonstrated by Klok and Oerlemans (2002) and Pellicciotti and others (2005). Relative humidity is not taken into account directly in EB1, as opposed to EB2, in which incoming longwave radiation is modelled

DOI: 10.1002/hyp

from air temperature and precipitable water, which, in turn, is a function of screen air temperature and vapour pressure (Prata, 1996). This distinction seems crucial in view of two factors: (1) in this climatic setting clouds are rare, and therefore overestimation of cloud cover has a stronger impact; (2) parameterizations based on cloud amount or fractional cloud cover can be inaccurate (Klok and Oerlemans, 2002), also in light of the difficulties discussed above in determining accurate cloud factor from comparison of measurements and simulations at the hourly scale. Niemelä and others (2001) have conducted a comprehensive evaluation of several parameterizations and showed that the equations proposed by Prata (1996) are among the most accurate, especially for dry climates. Simulations with EB1 in which the cloud factor was set to 1 in the night hours show indeed an increase of the incoming longwave flux from 269 to 306 W m^{-2} (Table IV). This results in an overestimation of total ablation at the end of the season (with a total ablation of 4310 mm w.e. simulated by EB1 with cloud factor of 1 at night), suggesting that correct modelling of the incoming longwave flux might be more important than consideration of the heat conduction into the snowpack, at least at this elevation.

Figure 10 shows the daily mean fluxes computed with EB2 over the period of record, together with the daily ablation simulated by the model. The largest flux in this period is incoming shortwave radiation, with a daily average of 344 W m^{-2}, followed by the outgoing longwave radiation (daily average of 306 W m^{-2}). This is in contrast with several energy balance studies that have shown that the highest single flux is the outgoing longwave radiation (e.g. Ohmura, 2001; Greuell and Smeets, 2001; Klok and others, 2005), and confirms that at these latitudes incoming shortwave radiation is extremely high. It is also the flux that shows the strongest diurnal variation (Figure 11).

The sensible heat fluxes are always positive over the period of record, with an average daily value of 56 W m^{-2} (Table IV). Their high values at the end of January and beginning of February are associated with the high temperatures observed in that period at AWS1 (Figure 3). Latent heat fluxes are negative (daily average is -19 W m^{-2}), in agreement with findings of other studies on various glaciers both in the Alps and Andes van de Wal and others 1992; Wagnon and others, 1999a; Carenzo and others, 2008). Net longwave radiation is always negative over the period of record (daily average is -54 W m^{-2}), in agreement with observations across latitudes and elevations (e.g. Greuell and Smeets, 2001; Carenzo and others, 2008), while the net solar radiation is positive and is the largest flux contributing to the surface-energy balance. Variations of the net shortwave radiation flux over the ablation season are clearly dominated by variations in albedo (see Figure 5): the increase in ablation from beginning of January onwards corresponds to the decay in albedo from the values typical of snow to the low ice albedo reached on 14 January (Figure 5). Ablation rates almost double accordingly (Figure 10c), and stay high until the snowfall of 12 February. One can also distinguish the four overcast days over the measurement period: 21 December, 1 and 22 January and 11 February, in both the shortwave radiation flux record and the simulated ablation (Figure 10c).

Figure 11 depicts the mean diurnal cycle of the single energy fluxes. Shortwave radiation (both incoming and reflected) reveals the strongest diurnal fluctuations. Both incoming and outgoing longwave radiation exhibit daily variations (which can be appreciated only partly in Figure 11 because of the scale of the y-axis): the outgoing flux increases around 8:00, in association with the warming up of the surface, the temperature of which rises again to melting point in the morning (see Figure 9), then remains stable (surface at melting point) and decreases slightly again around 18:00 because of the cooling of the surface to below zero values. A very similar behaviour of the outgoing longwave flux was observed also by Favier and others (2004a) on Antizana Glacier. The incoming longwave flux shows a maximum in the afternoon, as in Greuell and Smeets (2001); Favier and others (2004a); Klok and others (2005).

Sensible heat fluxes are always positive during the day, with a clear daily cycle showing a maximum in the afternoon associated with the daily variation of atmospheric temperature and wind speed (see Figure 4) (Greuell and Smeets, 2001). These maxima are not present when daily variations in wind speed are small (Klok and others, 2005), which however was not the case in this study, since winds showed a clear maximum in the afternoon (Figure 4).

The averaged hourly incoming shortwave radiation is much higher than that observed in the Alps (compare it with Figure 5 of Greuell and Smeets (2001) for the Pasterze glacier in Austria and with Carenzo and others (2008) for Haut Glacier d'Arolla), mainly due to the absence of overcast conditions. Mean values of daily incoming shortwave radiation over a period of 64 days in the ablation season for Haut Glacier d'Arolla and Gornergletscher in the Swiss Alps were 178 (Arolla in 2001), 204 (Arolla in 2005), 220 (Arolla in 2006), 240 (Gorner in 2005) and 241 W m^{-2} (Gorner in 2006), respectively, in contrast with a mean value of 344 W m^{-2} on Juncal (Table IV). Although topographic conditions, and especially shading, at the AWSs might differ from glacier to glacier, these values nevertheless give an indication of the much higher shortwave radiation receipt on Juncal Norte Glacier. Some corresponding mean values of daily ablation are: 38 (Arolla in 2005), 44 (Arolla in 2006), 48 (Gorner in 2005) and 48 mm w.e. (Gorner in 2006), as compared to a mean value of 58 mm w.e. computed at AWS1 by EB2.

Enhanced temperature-index model

In Figure 7, cumulative ablation computed by the two energy balance models is compared with ablation

DOI: 10.1002/hyp

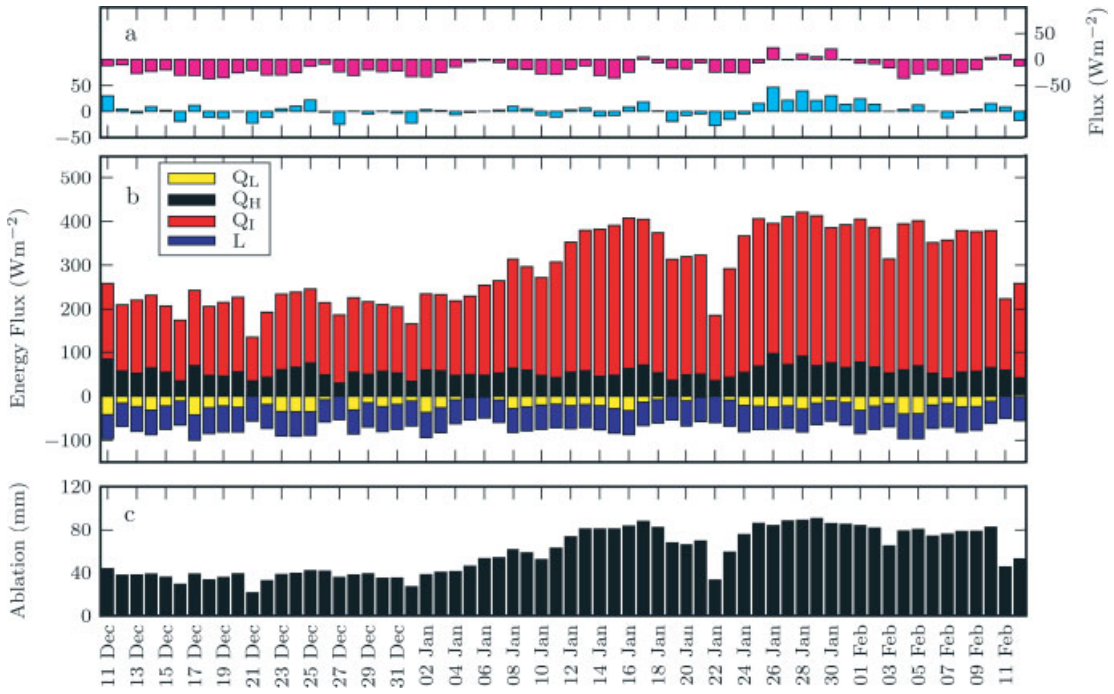

Figure 10. (a) and (b) daily means of the energy fluxes: (b) net shortwave radiation flux (Q_I), net longwave radiation flux (L), sensible (Q_H) and latent (Q_L) heat fluxes computed by EB2 at AWS1 for the entire period of record; (a) ($Q_H + L$) (cyan) and ($Q_H + Q_L + L$) (magenta). (c) daily ablation

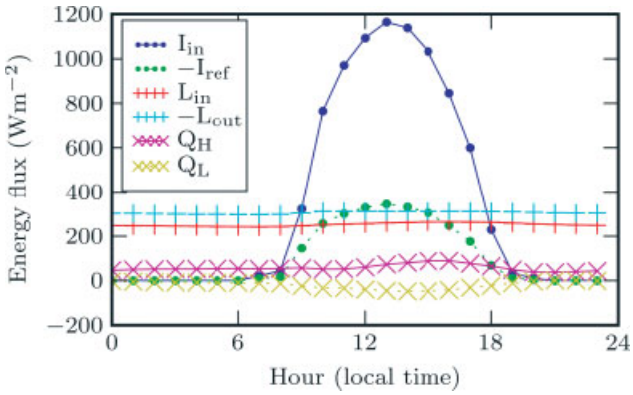

Figure 11. Mean daily cycle of the components of the surface energy balance at AWS1 computed by EB2: incoming (I_{in}) and reflected (I_{ref}) shortwave radiation; incoming (L_{in}) and outgoing (L_{out}) longwave radiation; sensible (Q_H) and latent (Q_L) heat fluxes. The hourly values are averages over the period of record (11 December 2005–12 February 2006)

simulated by the ETI model with values of parameters recalibrated at the location of AWS1. Both simulations with values of parameters typical of the Alps and recalibrated at the location of AWS1 were conducted and the model parameters and corresponding efficiency criterion R^2 are listed in Table V. In the first case, the parameters are taken from a recent study on the ETI model transferability that assessed the robustness of the parameters for a number of locations and seasons on three glaciers in the Alps (Carenzo and others, 2008). In the second case, the parameters were recalibrated against ablation rates simulated by EB2, which proved to correctly represent the ablation processes typical of this climatic setting.

The ETI model with parameters' values for the Alps overestimates cumulative ablation predicted by EB2 by about 235 mm w.e. (Table V), whereas recalibration of model parameters leads to a good agreement between ETI model and EB2 simulations (Figure 7 and Table V). Recalibration of model parameters results in a negative *TF*, and in a much higher *SRF* when compared to the values from the Alps case studies (Table V). The *SRF* nears its physically based value of 0·01078, which corresponds to the conversion factor from units of W m^{-2} to mm w.e. h^{-1} (Pellicciotti and others, 2005; Carenzo and others, 2008), reflecting the much higher contribution of solar radiation to the total melt in these latitudes.

Negative values of the *TF* indicate a net average negative contribution of the temperature-dependent terms of the energy balance (longwave radiation and turbulent sensible fluxes) to the total energy available for melt. Such negative contribution is mainly associated with the loss of energy by the glacier surface that is due to the radiative cooling, which is particularly strong at night and is caused by low humidity values and absence of clouds (see discussion above and Figure 9).

Figure 10 shows, together with the single energy fluxes computed by EB2, also the sum of the temperature-dependent energy fluxes, Q_H and L (cyan), and the sum of Q_H, Q_L, and L (magenta). The three latter terms represent the not-radiation dependent terms in the energy balance equation (Equation (1)). Since in Equation (9) only the shortwave radiation balance is explicitly represented, the term ($Q_H + Q_L + L$) is taken into account by the temperature-dependent term on the right side of Equation (9), even though the latent heat flux is not directly dependent on temperature like Q_H and L. The

DOI: 10.1002/hyp

term ($Q_H + L$) is small (mean value over the period of record is 1 W m^{-2}), with both positive and negative values over the period of record (Figure 10). It is clearly positive only in the spell from 25 January to 2 February, when higher than average air temperatures (Figure 3) cause the sensible turbulent flux to be very high (Figure 10). Since the daily net longwave radiation flux is almost constant over the period of record (Figure 10), changes in ($Q_H + L$) are basically determined by variations in the sensible fluxes. The term ($Q_H + Q_L + L$), however, is almost always negative (with a mean value over the period of record of -17 W m^{-2}), thus explaining the negative value of the *TF* found in the recalibration of model parameters. This value, however, is close to zero, suggesting that, because the melting process is strongly dominated by solar radiation, the exact value of *TF* is not crucial, and that it could be set to zero. To test this assumption, we run the ETI model with the optimal *SRF* ($SRF = 0{\cdot}0106$) and $TF = 0$, and obtained a R^2 of 0·982, which differs from the one corresponding to the optimal parameters only on the fourth decimal (Table V). This confirms that assuming a zero *TF* does not degrade the model performance in any significant manner.

Figure 12 shows couples of optimal model parameters computed for a number of locations and seasons on three glaciers in the European Alps (from Carenzo and others, 2008), together with the optimal parameters obtained from recalibration at AWS1 against EB2 simulations. The optimal parameters for Juncal are remarkably distinct from those for the Alps, as discussed above, in particular for the negative *TF*. No negative values were obtained for the two glaciers and three seasons considered in Carenzo and others (2008), reflecting the fact that frequent overcast conditions in the Alps reduce radiative cooling (therefore reducing the negative longwave radiation flux) (see Carenzo and others, 2008, for a complete discussion on this point). Under such conditions, the total contribution of the temperature-dependent term in Equation (9) is positive. Our finding is in agreement with the results of Carenzo and others, (2008), who have analysed the values of the model parameters for clear-sky and overcast conditions separately, and have found that *TF* increases under overcast conditions and is lower and close to zero for clear-sky conditions. Carenzo and others (2008) also obtained higher *SRF*s for clear-sky days than for the entire ablation season (with 48% of overcast days over the total measuring period) for a location on Haut Glacier d'Arolla.

Table V. Empirical parameters and efficiency criterion R^2 obtained at AWS1 using values of parameters typical of the Alps (from Pellicciotti and others (2005) and Carenzo and others (2007)) and recalibrated at AWS1 against simulations of hourly ablation with EB2 over the entire period of record. Total ablation *M* calculated by the ETI model with the two parameters' sets is also reported. Differences in ablation are computed with respect to the total ablation simulated by EB2

	Alps	Juncal Norte	Units
TF	0·04	−0·01	mm h^{-1} °C^{-1}
SRF	0·0094	0·0106	m^2 mm W^{-1} h^{-1}
R^2	0·966	0·982	—
M	3930	3746	mm w.e.
Difference	6·3	1·4	%

CONCLUDING REMARKS

In this paper, we used data from AWSs to study the components of the energy balance on a glacier in the semi-arid Andes. We also applied ablation models of different complexity, in particular a surface energy balance model, which makes use of the zero-degree assumption; a more complex energy balance model that considers the heat conduction through the snow or ice pack using a two-layer model; and an enhanced temperature-index model including the shortwave radiation balance. By using the two energy balance models, we intend to investigate the physical processes that govern ablation at these latitudes, as the meteorological forcing is distinct from that of other climatic settings such as the European Alps. By applying the enhanced temperature-index model, our aim is to investigate whether such a model is suitable for these climatic conditions and how these affect the model empirical parameters. Motivation for doing so is that the model empirical parameters were shown to be relatively robust for a range of meteorological conditions and location characteristics in the European Alps. We do not want to affirm that one type of model is better than the other, but rather provide a range of applicability, together with an evaluation of their respective accuracy and limitations, for both approaches. While energy balance models can be more accurate than temperature-index methods (and especially so than the simple standard approach), simplifications in the melt equations can be useful because of lack of data, for studies of melt regime over several seasons or for using observations outside the glacier boundary layer.

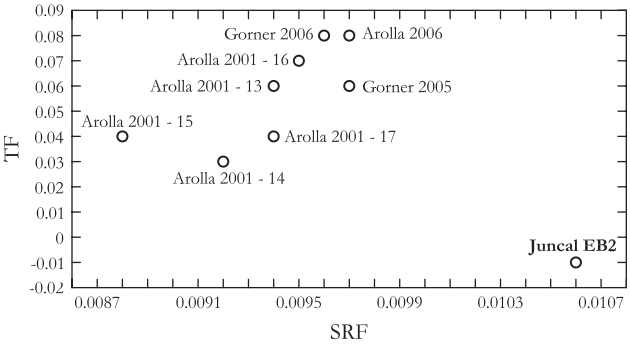

Figure 12. Optimal values of *TF* and *SRF* in the parameters' space for Juncal Norte Glacier (in red) and for the study sites and seasons examined in Carenzo *et al.* (2007) for the European Alps. The labels 'Arolla' and 'Gorner' indicate Haut Glacier d'Arolla and Gornergletscher, respectively. The numbers next to 'Arolla' designate different AWSs (see Carenzo *et al.* (2007) for a detailed explanation). *TF* and *SRF* are expressed in mm h^{-1} °C^{-1} and m^2 mm W^{-1} h^{-1}, respectively

DOI: 10.1002/hyp

We also carried out a thorough analysis of meteorological data on and close to the glacier to understand the meteorological forcing on this glacier in the semi-arid Andes of central Chile. The factors driving the ablation process in this climatic setting, as determined from analysis of the record of meteorological variables, exhibit distinct characteristics as compared to those in the European Alps. In particular, precipitation is close to zero during summer, and therefore albedo variations are limited apart from the change corresponding to the transition from snow to ice. Relative humidity is low and overcast conditions very rare, resulting in very high incoming solar radiation. As a consequence, there is no need for some of the parameterizations commonly used in the Alps in melt modelling, including albedo and cloud cover parameterizations. Both variables, and cloud cover in particular, represent a source of uncertainties in melt modelling (Klok and Oerlemans, 2002; Pellicciotti and others, 2005), especially at the distributed scale, and numerous parameterizations with various degrees of complexity have been developed and implemented in numerical models of glacier melt (e.g. Oerlemans, 1993; Greuell and Konzelmann, 1994; Oerlemans and Knap, 1998; Dai and others, 1999; Brock and others, 2000a; Pellicciotti and others, 2005).

This work has also shown that the ablation process is dominated by incoming shortwave radiation, confirming findings by other authors (e.g. Corripio, 2003). It has also demonstrated, however, that it is important to take into account the strong radiative cooling of the glacier surface due to the dry and cloud-free atmosphere. This is important both in energy balance models and in the ETI approach (by means of appropriate values of parameters).

Inclusion of the heat conduction and corresponding recomputation of the glacier- surface temperature is important for the correct estimation of ablation rates and total ablation. Using the zero-degree assumption leads to overestimation of ablation since part of the energy that the model uses for melt is in reality needed to warm up the snowpack to melting point. Neglecting the heat exchange between the surface and the snow or ice pack lead to an overestimation of about 75 mm w.e. (corresponding to 2% of the total ablation) at the location of our AWSs over a period of 64 days, and it is likely to be more important at higher elevations. This process is relevant in this climatic setting due to the low relative humidity and related absence of clouds that favour a very efficient radiative cooling especially at night and in the early hours of the morning. An effort, however, could be made to extend the findings of this work to other climatic contexts and locations, including the Alps, in order to test under which conditions the zero-degree assumption can effectively be used. Modelling the heat conduction flux into the snowpack is included in some existing energy balance models but not in others. Among the former, are studies by Greuell and Konzelmann (1994); Wagnon and others, (1999a); Klok and Oerlemans (2002). Among the latter, are the works of Hock and Noetzli (1997); Brock and Arnold (2000); Willis and others (2002); Favier and others (2004a); Corripio and Purves (2005). A recent work by Carenzo and others (2008) has looked at the validation of the energy balance model by Brock and Arnold (2000) (EB1 in this study) in the Swiss Alps. The model was tested over several seasons at the location of AWSs on two different glaciers, and results showed that the model simulations agree very well with observations at both ablation stakes and UDG. In contrast to this, we show that the model overestimates ablation in the semi-arid Andes, and that inclusion of the heat conduction is important under this climatic setting. Since evidence from different case studies is not conclusive, further research could be devoted to extend these findings.

We have also proved, that, at least at the elevation of AWS1, a major source of overestimation of ablation rates by EB1 is due to the computation of the incoming longwave radiative flux. Our finding supports previous evidence provided by Greuell and Smeets (2001) that incoming longwave radiation was the major source of uncertainty in point-scale energy balance modelling on Pasterze glacier, Austrian Alps. Under the climatic conditions typical of the dry Andes, characterized by almost constant cloud-free sky, the choice of the correct incoming longwave radiation model, among the several ones existing in the literature (e.g. Arnold and others, 1996; Greuell and others, 1997; Brock and Arnold, 2000), is crucial. In particular, we suggest that in this climatic setting a parameterization based on precipitable water, i.e. on both screen air temperature and vapour pressure, works better than one based on the more traditional cloud cover or cloud amount, computed from the ratio of measured and modelled clear-sky solar radiation, such as those used by Greuell and others (1997); Greuell and Smeets (2001); Klok and Oerlemans (2002). A similar result was obtained also in the comparative study carried out by Niemelä and others (2001). Klok and Oerlemans (2002) have shown that an overestimation of cloud cover leads to a significant increase in modelled ablation, whereas underestimation of cloud cover does not influence ablation substantially. Our results confirm this evidence, since both EB1 versions overestimated measured ablation. Our experiment with night cloud factors set to 1 showed that the model simulations are indeed very sensitive to overestimation of the value of the cloud factor (and related changes in the incoming longwave radiation), by showing a considerable overestimation of total ablation due to higher than in reality prediction of overcast conditions. Pellicciotti and others (2005) have suggested that derivation of cloud amount from the ratio of shortwave radiative fluxes at hourly resolution is likely to bring further errors, due to the difficulty of matching measurements and model predictions in the early morning and late afternoon hours, when effects such as shading and inaccuracies of the sensor due to low zenithal angles make the values differ although peak hours agreement might be very good.

DOI: 10.1002/hyp

This work has also demonstrated that ETI models or simplified energy balance approaches can also be used, but that simple extrapolation to a different climatic setting is not appropriate, since the model empirical parameters need to reflect the distinct processes taking place in such climatic setting. In particular, we have demonstrated that the higher solar radiation input results in a higher contribution from the shortwave radiation flux and therefore a higher *SRF*, which becomes very close to its physically based value. The strong radiative cooling, especially at night, causes a reduction in the energy available for melt in the first hours of the day, since this is necessary to heat up the snow or ice pack. As a consequence, the contribution from the temperature-dependent fluxes is zero or negative, and the optimal *TF* also assumes negative values. We suggest, however, that once the ETI model is adapted to the climatic setting, it can be successfully used, because it is more physically based than the standard temperature-index method, and its parameters have a clearer physical meaning (Carenzo and others, (2008). The two model parameters indeed change in response to variations in the relative contribution of the single fluxes of the energy balance, as it is suggested by comparison with the parameters' values obtained for Alpine glaciers. We have also shown that, once the correct range of the values of parameters corresponding to the specific climatic setting has been identified, variations in *TF* are not of crucial importance, because of the little sensitivity of the model to changes in this parameter. Simulations with $TF = 0$ lead to a very small decrease in model performance, suggesting that a *TF* of zero could also be used with little error, at least for simulations at the point scale. The impact of the use of different *TFs*, however, should be tested in the distributed application of the model to the entire glacier.

Although numerous current studies of glacier ablation focus on simulation of melt at the distributed scale across an entire glacier (e.g. Arnold and others, 1996; Klok and Oerlemans, 2002; Hock and Holmgren, 2005), studies at the point scale are still relevant for the understanding of the processes of interaction between climate and glaciers. Recent examples of studies at the point scale are, among others, those of Greuell and Smeets (2001); Favier and others (2004a); van den Broeke and others (2004); Klok and others (2005); Pellicciotti and others (2005). They allow investigating the relationship between the climate and the glacier-surface energy balance using direct meteorological observations at AWSs. In distributed modelling, on the contrary, the need to extrapolate the input meteorological variables to the grid cells lead to uncertainties introduced by the parameterizations of input variables such as air temperature, solar radiation and albedo. Point-scale studies, therefore, still represent a crucial step preliminary to the extrapolation of the energy balance and melt modelling to the glacier-wide scale. This paper has contributed to the understanding of the ablation processes at the point scale using meteorological and ablation data collected on Juncal Norte Glacier, in climatic conditions previously little investigated. In a next paper, we will look at the distributed application of both the EB2 and ETI model.

We have also shown that measurements at the proglacial station are affected by the katabatic wind that was observed at AWS1. Temperature fluctuations are similar at the two stations, although those at AWS1 are less marked because of the well-known effect of the glacier in damping air temperature in the glacier boundary layer. The diurnal cycle, however, was similar (Figure 4). Wind at both stations is affected by the glacier wind. Other studies have shown that AWSs located on valley slopes rather than in the proglacial field do exhibit distinct temperature and wind regimes from AWSs on glaciers (e.g. Klok and others, 2005). We intend to explore the applicability of the models used in this study with data from AWS2.

ACKNOWLEDGEMENTS

The authors would like to thank Jorge Quinteros for his assistance in the field, and Claudio Bravo, Karin Sepulveda, Roberto Garrido Cortes and Cesar Acuña for joining some of the field expeditions. Ružica Dadić provided valuable help in the field and with the instrumentation. The field work in Chile was partly funded by the Geneva International Academic Network (GIAN). The Department of Security, Health and Environment (Abteilung fuer Sicherheit, Gesundheit und Umwelt) of ETH Zurich provided both equipment and funding for the field expedition. In Chile, many individuals were supportive of our work, among these a particular thanks goes to Monica Rodriguez. The comments of Patrick Wagnon and an anonymous reviewer on the early version of the manuscript were very useful and are gratefully acknowledged. Thanks also to the scientific editor Regine Hock.

REFERENCES

Andreas EL. 1987. A theory for the scalar roughness and the scalar transfer coefficients over snow and sea ice. *Boundary-Layer Meteorology* **38**: 159–184.

Arnold NS, Willis IC, Sharp MJ, Richards KS, Lawson WJ. 1996. A distributed surface energy balance model for a small valley glacier. I. Development and testing for Haut Glacier d'Arolla, Valais, Switzerland. *Journal of Glaciology* **42**(140): 77–89.

Bown F, Rivera A Acuña C. 2008. Recent glaciers variations at the Aconcagua basin, central Chilean Andes. *Annals of Glaciology* **48**: 43–48.

Braithwaite RJ, Konzelmann T, Marty C, Olesen OB. 1998. Reconnaissance study of glacier energy balance in North Greenland, 1993–94. *Journal of Glaciology* **44**(147): 239–247.

Braithwaite RJ, Olesen OB. 1990. A simple energy balance model to calculate ice ablation at the margin of the Greenland ice sheet. *Journal of Glaciology* **36**(123): 222–228.

Brock BW, Arnold NS. 2000. A spreadsheet-based (Microsoft Excel) point surface energy balance model for glacier and snowmelt studies. *Earth Surface Processes and Landforms* **25**: 649–658.

Brock BW, Willis IC, Sharp MJ. 2000a. Measurement and parameterisation of albedo variations at Haut Glacier d'Arolla, Switzerland. *Journal of Glaciology* **46**(155): 675–688.

Brock BW, Willis IC, Sharp MJ, Arnold NS. 2000b. Modelling seasonal and spatial variations in the surface energy balance of Haut Glacier d'Arolla, Switzerland. *Annals of Glaciology* **31**: 53–62.

Brock BW, Willis IC, Sharp MJ. 2006. Measurement and parameterization of aerodynamic roughness length variations at Haut Glacier d'Arolla, Switzerland. *Journal of Glaciology* **52**(177): 281–297.

Cai X, Rosegrant MW, Ringler C. 2003. Physical and economic efficiency of water use in the river basin: Implications for efficient water management. *Water Resources Research* **39**(1): 1013.

Carenzo M, Pellicciotti F, Rimkus S, Burlando P. under revision. Assessing the transferability and robustness of an enhanced-temperature index glacier melt model. *Journal of Glaciology*.

Carrasco J, Casassa G, Quintana J. 2005. Changes of the 0 isotherm and the equilibrium line in altitude in central Chile during the last quarter of the 20th century. *Hydrological Sciences Journal-Journal Des Sciences Hydrologiques* **50**(6): 933–948.

Corripio J. 2003. *Modelling the energy balance of high altitude glacierised basins in the Central Andes*. PhD thesis, University of Edinburgh.

Corripio JG, Purves RS. 2005. Surface Energy Balance of High Altitude Glaciers in the Central Andes: the Effect of Snow Penitentes, in *Climate and Hydrology in Mountain Areas*, de Jong C, Collins D, and Ranzi R (eds). Wiley & Sons: London.

Cutler P, Munro DS. 1996. Visible and near-infrared reflectivity during the ablation period on Peyto Glacier, Alberta, Canada. *Journal of Glaciology* **42**(141): 333–340.

Dai A, Trenberth KE, Karl TR. 1999. Effects of clouds, soil moisture, precipitation and water vapor on diurnal temperature range. *Journal of Climate* **12**: 2451–2473.

Denby B, Greuell W. 2000. The use of bulk and profile methods for determining surface heat fluxes in the presence of glacier winds. *Journal of Glaciology* **46**(154): 445–452.

Favier V, Wagnon P, Chazarin JP, Maisincho L, Coudrain A. 2004a. One-year measurements of surface heat budget on the ablation zone of Antizana Glacier 15, Ecaudorian Andes. *Journal of Geophysical Research* **109**: D18105. DOI: 10.1029/2003JD004359.

Favier V, Wagnon P, Ribstein P. 2004b. Glaciers of the outer and inner tropics: a different behaviour but a common response to climatic forcing. *Geophysical Research Letters* **31**: L16403. DOI: 10.1029/2004GL020654.

Francou B, Vuille M, Favier V, Caceres B. 2004. New evidence of an ENSO impact on low-latitude glaciers: Antizana 15, Andes of Ecuador, 0 28 S. *Journal of Geophysical Research* **109**: D18106, DOI: 10.1029/2003JD004484.

Greuell W, Böhm R. 1998. 2m temperatures along melting mid-latitude glaciers, and implications for the sensitivity of the mass balance to variations in temperature. *Journal of Glaciology* **44**(146): 9–20.

Greuell W, Knap WH, Smeets PC. 1997. Elevational changes in meteorological variables along a midlatitude glacier during summer. *Journal of Geophysical Research* **102**(D22): 25941–25954.

Greuell W, Konzelmann T. 1994. Numerical modelling of the energy balance and the englacial temperature of the Greenland Ice Sheet. Calculations for the ETH-Camp location (West Greenland, 1155 m a.s.l). *Global and Planetary Change* **9**(1–2): 91–114.

Greuell W, Smeets P. 2001. Variations with elevation in the surface energy balance on the Pasterze (Austria). *Journal of Geophysical Research* **106**(D23): 31717–31727.

Hock R. 1999. A distributed temperature-index ice- and snowmelt model including potential direct solar radiation. *Journal of Glaciology* **45**(149): 101–111.

Hock R, Holmgren B. 2005. A distributed surface energy balance model for complex topography and its application to Storglaciären, Sweden. *Journal of Glaciology* **51**(172): 25–36.

Hock R, Noetzli C. 1997. Areal melt and discharge modelling of Storglaciären, Sweden. *Annals of Glaciology* **24**: 211–217.

Klok EJ, Nolan M, van de Broeke MR. 2005. Analysis of meteorological data and the surface energy balance on McCall Glacier, Alaska, USA. *Journal of Glaciology* **51**(174): 451–461.

Klok EJ, Oerlemans J. 2002. Model study of the spatial distribution of the energy and mass balance of Morteratschgletscher, Switzerland. *Journal of Glaciology* **48**(163): 505–518.

Koh G, Jordan R. 1995. Sub-surface melting in a seasonal snow cover. *Journal of Glaciology* **41**(139): 474–482.

Kretz A. 2007. Modelling spatial and temporal variations in surface melt on Gornergletscher. Master thesis, VAW Zurich, ETH-Zürich, 110.

Lliboutry L. 1998. Glaciers of the Dry Andes, *in Satellite Image Atlas of Glaciers of the World SOUTH AMERICA*, Williams RSJ and Ferrigno JG (eds). United States Geological Survey Professional Paper 1386-I. Available onine: http://pubs.usgs.gov/prof/p1386i/index.html.

Masiokas M, Villalba R, Luckman B, Le Quesne C, Aravena J. 2006. Snowpack variations in the central Andes of Argentina and Chile, 1951–2005: Large scale atmospheric influences and implications for water resources in the region. *Journal of Climate* **19**(24): 6334–6352.

Montecinos A, Aceituno P. 2003. Seasonality of the ENSO-related rainfall variability in central Chile and associated circulation anomalies. *Journal of Climate* **16**: 281–296.

Munro DS. 1989. Surface roughness and bulk heat transfer on a glacier: comparison with eddy correlation. *Journal of Glaciology* **35**(121): 343–348.

Nash JE, Sutcliffe JV. 1970. River flow forecasting through conceptual models. Part 1. A discussion of principles. *Journal of Hydrology* **10**(3): 282–290.

Niemelä S, Räisänen P, Savijärvi H. 2001. Comparison of surface radiative flux parameterisations. Part I: Longwave radiation. *Atmospheric Research* **58**: 1–18.

Obukhov AM. 1971. Turbulence in an atmosphere with a non-uniform temperature. *Boundary-Layer Meteorology* **2**: 7–29.

Oerlemans J. 1993. A model for the surface balance of ice masses: part I. Alpine Glaciers. *Zeitschrift fur Gletscherkunde und Glazialgeologie* **27/28**(1991/1992): 63–83.

Oerlemans J, Knap WH. 1998. A 1 year record of global radiation and albedo in the ablation zone of Morteratschgletscher, Switzerland. *Journal of Glaciology* **44**(147): 231–238.

Ohmura A. 1981. *Climate and Energy Balance on Arctic Tundra*, vol. 3 of Zürcher Geographische Schriften. Geographical Institute of the Swiss Federal Institute of Technology: Zürich.

Ohmura A. 2001. Physical basis for the temperature-based melt-index method. *Journal of Applied Meteorology* **40**: 753–761.

Oke TR. 1987. *Boundary Layer Climates*, 2nd edn. Routledge: London.

Paterson WSB. 1994. *The Physics of Glaciers*, 3rd edn. Pergamon: New York.

Pellicciotti F. 2004. Development of an ice and snow melt model for long-term analysis of water resources from glacierised basins. PhD thesis, ETH Zürich.

Pellicciotti F, Brock B, Strasser U, Burlando P, Funk M, Corripio J. 2005. An enhanced temperature-index glacier melt model including the shortwave radiation balance: development and testing for Haut Glacier d'Arolla, Switzerland. *Journal of Glaciology* **51**(175): 573–587.

Pellicciotti F, Burlando P, van Vliet K. 2007. Recent trends in precipitation and streamflow in the Aconcagua River Basin, central Chile. *International Association of Hydrological Sciences* **318**: p. 17–38.

Peña H, Nazarala N. 1987. Snowmelt runoff simulation model of a central Chile Andean basin with relevant orographic effects, Large Scale Effects of Seasonal Snow Cover. *International Association of Hydrological Sciences* **166**: 161–172.

Prata AJ. 1996. A new, long-wave formula for estimating downward clear-sky radiation at the surface. *Quarterly Journal of the Royal Meteorological Society* **122**: 1127–1151.

Rimkus S. 2006. *Modelling distributed melt on Haut Glacier d'Arolla using an enhanced temperature-index approach: testing the model sensitivity and analysis of the spatial-temporal variability of the input data*. Master thesis, Institut of Environmental Engineering, ETH-Zurich, 104.

Rivera A, Acuña C, Casassa G. 2006. Glacier Science and Environmental Change, Blackwell, Oxford, UK, chap. Glacier variations in central Chile (32 °S–41 °S), 246–247.

Rivera A, Acuña C, Casassa G, Bown F. 2002. Use of remote sensing and field data to estimate the contribution of Chilean glaciers to the sea level rise. *Annals of Glaciology* **34**: 367–372.

Rivera A, Casassa G, Acuña C, Lange H. 2000. Variaciones recientes de glaciares en Chile. *Revista de Investigaciones Geograficas* **34**: 29–60.

Röthlisberger H, Lang H. 1987. Glacial Hydrology. In *Glacio-fluvial Sediment Transfer—An Alpine Perspective*, Gurnell AM, Clark MJ (eds). John Wiley and Sons: Chichester, New York, Toronto, Singapore; 207–284.

Sicart JE, Wagnon P, Ribstein P. 2005. Atmospheric controls of the heat balance of Zongo Glacier (16 Bolivia). *Journal of Geophysical Research* **110**: D12106, DOI:10.1029/2004JD005732.

van den Broeke MR. 1997. Structure and diurnal variation of the atmospheric boundary layer over a mid-latitude glacier in summer. *Boundary-Layer Meteorology* **83**(2): 183–205.

van den Broeke MR, Reijmer C, van de Wal RSW. 2004. A study of the surface mass balance in Dronning Maud Land, Antarctica, using automatic weather stations. *Journal of Glaciology* **50**(171): 565–582.

van de Wal RSW, Oerlemans J, van der Hage JC. 1992. A study of ablation variations on the tongue of Hintereisferner, Austrian Alps. *Journal of Glaciology* **38**(130): 319–324.

Wagnon P, Ribstein P, Francou B, Pouyaud B. 1999a. Annual cycle of energy balance of Zongo Glacier, Cordillera Real, Bolivia. *Journal of Geophysical Research* **104**(D4): 3907–3923.

Wagnon P, Ribstein P, Kaser G, Berton P. 1999b. Energy balance and runoff seasonality of a bolivian glacier. *Global and Planetary Change* **22**: 49–58.

Waylen P, Caviedes C. 1990. Annual and seasonal fluctuations of precipitation and streamflow in the Aconcagua River Basin, Chile. *Journal of Hydrology* **120**: 79–102.

Willis IC, Arnold NS, Brock BW. 2002. Effect of snowpack removal on energy balance, melt and runoff in a small supraglacial catchment. *Hydrological Processes* **16**(14): 2721–2749.